

Curvature Dependence of Hydrophobic Hydration Dynamics

R. Gregor Weiß,^{1,2} Matthias Heyden,³ and Joachim Dzubiella^{1,2,*}

¹*Department of Physics, Humboldt Universität zu Berlin, Newtonstr. 15, D-12489 Berlin, Germany*

²*Soft Matter and Functional Materials, Helmholtz-Center Berlin,
Hahn-Meitner Platz 1, D-14109 Berlin, Germany*

³*Max-Planck-Institut für Kohlenforschung, Kaiser-Wilhelm-Platz 1, D-45470 Mülheim an der Ruhr, Germany*

We investigate the curvature-dependence of water dynamics in the vicinity of hydrophobic spherical solutes using molecular dynamics simulations. For both, the lateral and perpendicular diffusivity as well as for H-bond kinetics of water in the first hydration shell, we find a non-monotonic solute-size dependence, exhibiting extrema close to the well-known structural crossover length scale for hydrophobic hydration. Additionally, we find an apparently anomalous diffusion for water moving parallel to the surface of small solutes, which, however, can be explained by topology effects. The intimate connection between solute curvature, water structure and dynamics has implications for our understanding of hydration dynamics at heterogeneous biomolecular surfaces.

One of the greatest advances in our understanding of the hydrophobic effect is the recognition that the hydration structure and thermodynamics of apolar solutes is qualitatively length scale dependent [1–11]. The microscopic reason is that water structures very differently at small (convex) solutes, where the bulk H-bond network is only moderately deformed, as compared to large solutes, which significantly distort the tetrahedral bulk structure. The structural crossover happens at sub-nanometer length scales and has important implications for the interpretation of the structure and thermodynamics of hydrophobically-driven assembly processes [1, 12], such as protein folding and association [13–15].

The dynamics of the hydration layer that surrounds molecular self-assemblies and proteins in solution has attracted plentiful interest in the last decade [16]. Solute fluctuations and hydration dynamics are understood to be highly coupled with important consequences to biological function, such as enzyme catalysis and molecular recognition in binding [16–26]. Despite the obvious importance of the solute chemical composition, apparently the intrinsic topological and geometric features play an important role as well [19–21, 27], possibly even leading to anomalous diffusion behavior [20]. Therefore, and due to the established fact that water considerably restructures at radii of curvature close to the sub-nanometer scale, a natural question to ask is, *how does the water structural crossover affect the dynamics of the hydration layers in the solute vicinity?*

One of the first simulation studies of curvature effects on hydration dynamics was performed by Chau *et al.* for three solute radii between 0.35 and 0.8 nm [28]. They found a slowdown of the diffusion of water in the first hydration shell relative to the bulk with an apparent minimum for the intermediate solute size. This interesting finding was not commented on, probably due to the little amount of data and statistical uncertainty of the results. Further, a slowdown of water reorientational dynamics was found compared to bulk, an effect that decreased with solute size [28]. The reorientational slowing-down

has been recently explained by excluded-volume effects on the H-bond exchange dynamics [29, 30]. In disagreement with the simulations with Chau *et al.*, however, the excluded-volume concept predicts a monotonic increase of the reorientation times [29], an apparent controversy which has not been addressed in literature, yet.

In this letter, we report on systematic molecular dynamics (MD) simulations of water around hydrophobic spherical model solutes of varying radius between 0.3 and 2.1 nm and investigate intrinsic curvature effects on water hydration dynamics. We find that the perpendicular and lateral diffusivity of hydration water exhibit a non-monotonic curvature dependence, with temperature-dependent minima located close to the structural crossover length scale [7, 31]. Both, curvature and temperature dependence, are strikingly similar to that of entropy during hydrophobic solvation [31] and thus allows strong conjecture that the hydrophobic effect extends beyond thermodynamic into dynamic anomalies. Furthermore, we find that the intriguing curvature dependence of the diffusivity is found to be related to a non-monotonic dependence of H-bond life times on curvature, exhibiting a maxima at the crossover length scale. This finding reconciles previous, apparently contradicting results from simulations [28] and theory [29, 30] on reorientation times, as we find both predicted behaviors but in different length scale regimes. The intimate connection between solute curvature and water structure and dynamics should be of fundamental importance for biomolecular function mediated by heterogeneous biomolecular surfaces [16, 17, 19–21, 27].

Our MD simulations are performed each containing a single and fixed hydrophobic model solute solvated in SPC/E water [32] using the Gromacs simulation package [33]. The solute-water interaction is mediated by a shifted Lennard-Jones potential $U_{LJ}(r') = 4\epsilon[(\sigma/r')^{12} - (\sigma/r')^6]$, whereas $r' = r - r_0$ describes a coordinate shift by r_0 . With such a shifted potential, it is guaranteed that by changing the solute size *only* intrinsic curvature effects are probed, not, e.g., those of an additionally vary-

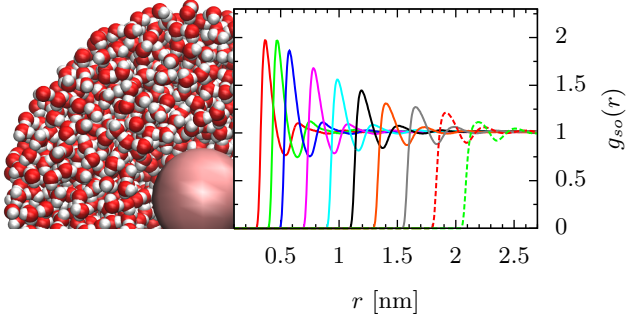


Fig. 1: Left: MD simulation snapshot of a hydrophobic sphere with shift radius $r_0 = 8 \text{ \AA}$ in explicit water. Right: Radial distribution function (RDF) $g_{so}(r)$ of water around differently sized hydrophobic model solutes.

ing dispersion attraction. Values of $\sigma = 3.768 \text{ \AA}$ and $\epsilon = 1.197 \text{ kJ/mol}$ are chosen from a model for methane to mimic a reasonable dispersion attraction with a well-defined first solvation shell [6]. We choose shift radii $r_0 = 0 \text{ \AA}, 1 \text{ \AA}, 2 \text{ \AA}, 4 \text{ \AA}, 6 \text{ \AA}, 8 \text{ \AA}, 10 \text{ \AA}, 12.5 \text{ \AA}, 15 \text{ \AA}$ and 17.5 \AA in ten separate simulations. As a limiting case of a hydrophobic surface with zero curvature, the box delimiting walls in the $x-y$ -plane in a pseudo-2D simulation are chosen to interact with water by a 12-6 potential in z -direction $U_{12-6}(z) = 4\epsilon[(\sigma/z)^{12} - (\sigma/z)^6]$. After 100 ps of Gibbs ensemble (NPT) equilibration, canonical (NVT) production runs are performed up to 200 ns at a temperature of $T = 300 \text{ K}$ and with $N = 6000$ to 12000 water molecules. Further details on the simulation technique can be found in the Supporting Information (SI). A simulation snapshot and water oxygen density profiles around all the solutes are presented in Fig. 1.

We first characterize the water diffusion parallel to the solute surface. For this, we calculate the lateral mean square displacement (MSD) of the arc length a water oxygen has traveled in time t , via

$$\langle S(t)^2 \rangle = R_{\text{avg}}^2 \cdot \langle [\theta(t' + t) - \theta(t')]^2 \rangle_{R_1}. \quad (1)$$

Here $R_{\text{avg}} = \int_0^{R_1} dr r \cdot g_{so}(r)$ denotes the average distance of the water molecules inside the first hydration layer, which is delimited by the location R_1 of the first minimum in the RDF (cf. Fig.1), to the solute center. The time average $\langle \dots \rangle_{R_1}$ over starting times t' is taken only in the first hydration shell. The variable $\theta(t)$ is the azimuthal angle of the water oxygen-solute distance vector at time t . For water molecules diffusing at a wall, Eq.(1) reduces to the usual two dimensional MSD $\langle [\Delta x(t) + \Delta y(t)]^2 \rangle_{R_1}$ in the $x-y$ -plane.

The lateral MSDs for water around all solutes are shown in Fig. 2(a) along with those of water at the planar hydrophobic surface and in bulk. Comparison to the bulk MSD indicates a crossover from below to above bulk water self-diffusion with increasing slopes with growing so-

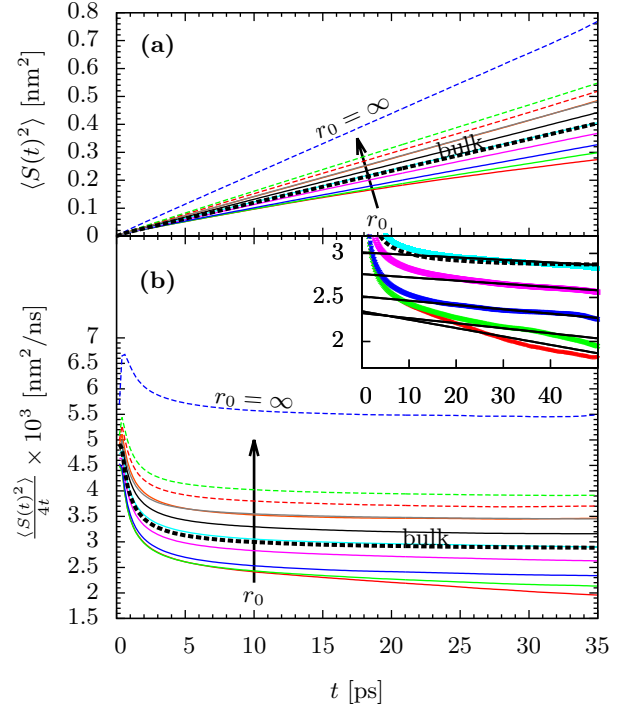


Fig. 2: (a) MSD of water molecules parallel to differently curved hydrophobic surfaces and MSD of water in bulk (thick black dashed line). (b) The data from the top panel (a) divided by $4t$. The *Inset* shows the curves for water at the five smallest solutes along with the corresponding fits from Eq. (3).

lute size. Additionally, the hydrating water of the smallest solutes exhibits non-linear, anomalous behavior in t . This can be better recognized by the negative slope for small solutes in Fig. 2(b) where we plot the MSD divided by time, $\langle S(t) \rangle / 4t$. Linearity of the MSDs is restored for larger solutes, converging towards the limiting MSD $r_0 \rightarrow \infty$ of the planar hydrophobic surface.

The apparently anomalous diffusion behavior for small solutes can be explained by intrinsic curvature effects, which modify the standard 2D diffusion law [34]. Here, the probability distribution function (PDF) of diffusion on spherical surfaces reads

$$P(\theta, \tau) = \frac{N(\tau)}{\tau} \sqrt{\theta \sin(\theta)} \cdot e^{-\frac{\theta^2}{2\tau}} \quad (2)$$

where $\tau = 2D_{||}t/R_{\text{avg}}^2$, and $N(\tau)$ is a normalization constant. By expanding Eq. (2) up to second order for small θ , we find that the second moment of the PDF can be written for small solutes as

$$\langle \theta^2 \rangle R_{\text{avg}}^2 \approx 4D_{||}t - \frac{4}{3} \frac{D_{||}^2 t^2}{R_{\text{avg}}^2}. \quad (3)$$

On surfaces with high curvature ($R_{\text{avg}}^2 \ll D_{||}t$) the second term on the r.h.s. of Eq. (3) slows down the MSD

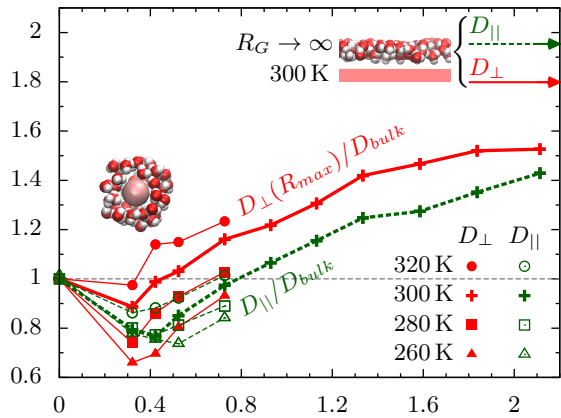


Fig. 3: Parallel and perpendicular diffusivities D_{\parallel} (green dashed lines) and D_{\perp} (red solid lines) scaled by bulk water diffusion D_{bulk} against solute size R_G for $T = 300$ K. For the four smallest cavities the temperature effect on D_{\perp} and D_{\parallel} is shown for $T = 260$ K, 280 K and 320 K. The grey dashed horizontal line represents bulk water diffusivity. The values corresponding to diffusivity at the limiting case of zero curvature ($R_G \rightarrow \infty$, only $T = 300$ K) are drawn as horizontal arrows with respective color coding.

as found in our simulations. In the limit $R_{avg} \rightarrow \infty$, this term vanishes and the MSD on planar surfaces, $\propto 4D_{\parallel}t$, is restored, consistent with the vanishing non-linearity as observed in Fig. 2.

By fitting Eq. (3) to our MSDs, we obtain the lateral diffusion constant D_{\parallel} , see the inset in Fig. 2(b) for the fits. The results are plotted versus the Gibbs radius of the solutes in Fig. 3 at $T = 300$ K normalized by bulk diffusion constant D_{bulk} of water. For small solutes, we find that the parallel diffusion D_{\parallel} slows down with increasing solute sizes which leads to parallel mobilities smaller than in bulk. This trend changes at a minimum at a length scale of $R_G^* \approx 0.45$ nm beyond which the lateral diffusivity monotonically rises with decreasing surface curvature to become bulk-like at about $R_G^* \approx 0.75$ nm and finally saturates to a water mobility higher than in bulk, as well known for smooth and planar hydrophobic surfaces [35]. The significant length scales observed here match well the structural crossover length scale of ≈ 0.5 nm found for SPC/E water estimated from solvation free energies of spherical model solutes [7].

To calculate the water diffusivity *perpendicular* to the hydrophobic surfaces, we employ the mean first-passage time (MFPT) analysis introduced by Hinczewski *et al.* [36, 37]. The MFPT $T_{fp}(r, r_t)$ describes the mean time required by a molecule to travel from distance r to the solute to a target distance $r_t > r$ and has an exact solution in a Smoluchowski description in terms of the free energy $F(r)$ and diffusivity profile $D_{\perp}(r)$ [38]. Its inversion leads to an expression for the perpendicular diffusivity

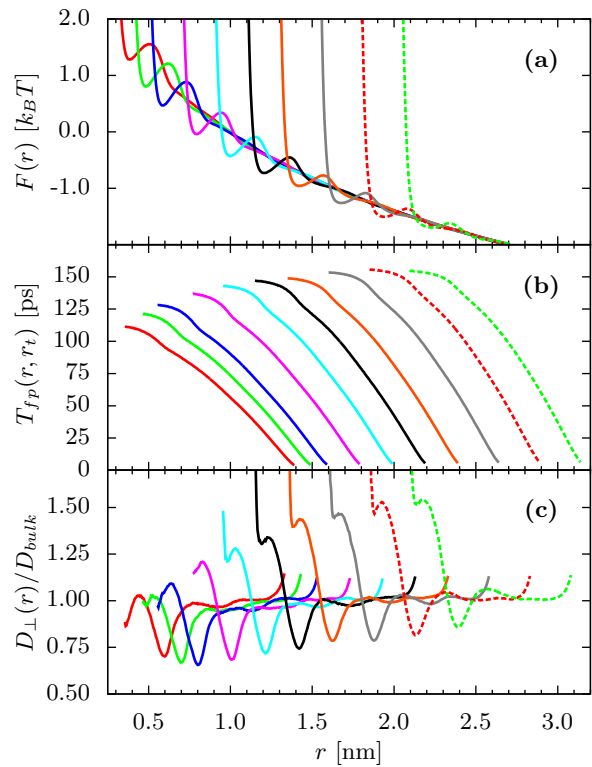


Fig. 4: (a) Free energy profile $F(r)$ for water around differently sized hydrophobic solutes obtained by the Boltzmann inversion of the water RDFs in Fig. 1. (b) MFPT curves $T_{fp}(r, r_t)$ for water molecules to reach the target distance at $r_t = 14$ Å given they started at a distance $r < r_t$. (c) Perpendicular diffusivity profiles $D_{\perp}(r)$ obtained from Eq. (4).

profile [36, 37]

$$D_{\perp}(r) = -\frac{e^{\beta F(r)}}{\partial T_{fp}(r, r_t)/\partial r} \int_{r_{min}}^r dr' e^{-\beta F(r')} \quad (4)$$

with $\beta^{-1} = k_B T$ and r_{min} being a reflective boundary close to the solute where $F(r_{min}) = 10 k_B T$. From our MD simulations, we extract MFPTs $T(r, r_t = r_0 + 14$ Å) as shown in the middle panel (b) of Fig. 4 along with free energy profiles $F(r)$ in the upper panel (a). The latter result from a simple Boltzmann inversion of the solute-water RDFs plus the entropic contribution $F(r) = -k_B T \ln g_{so}(r) - 2k_B T \ln r$ [37]. The bottom panel (c) plots the resulting diffusivity profiles $D_{\perp}(r)/D_{bulk}$ normalized by bulk diffusivity for all solute sizes. The general shape of the profiles describes a maximum inside the first solvation shell followed by a minimum in diffusivity which is reached at the outside margin of the solvation layer, whereafter diffusivity converges towards bulk diffusion in an oscillatory fashion. (The final rise of the profiles for radii close to the target distance is an artifact of non-Markovian contributions [36, 37], see also the SI for technical details.) In our calculated profiles, an interesting non-monotonic curvature dependence of the

perpendicular water mobility near hydrophobic surfaces is visible in the extrema of the profiles. With growing solute size, the maximum of diffusivity in the first hydration shell continues to increase which leads to high perpendicular diffusivity in vicinity of weakly curved surfaces, whereas the minimum becomes less pronounced and almost vanishes in the profile at the planar limit (see SI).

We now define the perpendicular diffusion coefficient $D_{\perp}(R_{max})$ in the first hydration shell by the value of the diffusivity curve at R_{max} , the position of the first peak of the RDF. The scaled value $D_{\perp}(R_{max})/D_{bulk}$ is presented next to the scaled values of D_{\parallel} in Fig. 3 versus solute size R_G for $T = 300$ K. Like D_{\parallel} , the perpendicular diffusivity also shows the crossover from below-to-above bulk mobility, but at a smaller distance of about 0.4 nm, indicating a preceding non-monotonic solute size dependence for small solutes as it is interpolated towards the limiting (bulk) case of a solute with vanishing radius. Since the magnitude of the perpendicular diffusivity slightly depends on the definition of what radius defines the first hydration shell, or if over all water molecules in this shell should be averaged, we compare those different definitions in the SI. We find similar values, in particular, all tested definitions rigorously reproduce the crossover from below-to-above bulk mobility behavior of water versus solute size close to the structural crossover length scale.

Additionally Fig. 3 plots diffusivity changes upon three different temperatures $T = 260$ K, 280 K and 320 K at cavities at which the dynamic anomaly occurs. Decreasing temperature shifts the curves and the dynamic anomaly towards larger radii of curvature. Hence, the observed temperature dependence of diffusive dynamics obeys the same trend as the thermodynamic and structural crossover length scale [31]. Taking into account entropy scaling laws for diffusion [39, 40], which scale exponentially with excess entropy, suggests entropy to be a constitutive measure for the dynamic anomaly, thus firmly corroborating our conclusions.

Ultimately, water hydrogen bond (HB) kinetics and mobility are intimately linked because translational diffusion is accompanied by processes breaking, forming and re-forming HBs. The cooperation of elemental dynamic processes in water is successfully described with reaction-diffusion models [41–43] and was probed by simulations [41–44]. Here, we probe HB lifetimes τ which are estimated by the correlation function $c(t) = \langle h(t)h(0) \rangle / \langle h^2 \rangle$ of the HB operator $h(t)$, which is 1 for a specific pair of water molecules while they are bonded, and 0 otherwise [41–43]. The negative derivative $k(t) = -dc(t)/dt$ is the reactive flux hydrogen bond correlation function. We estimate 'intermittent' HB lifetimes by the zero frequency part [42], the integral of $c(t)$,

$$\tau = - \int_0^{\infty} t \cdot k(t) dt = \int_0^{\infty} c(t) dt . \quad (5)$$

It is significantly influenced by diffusion leading to the

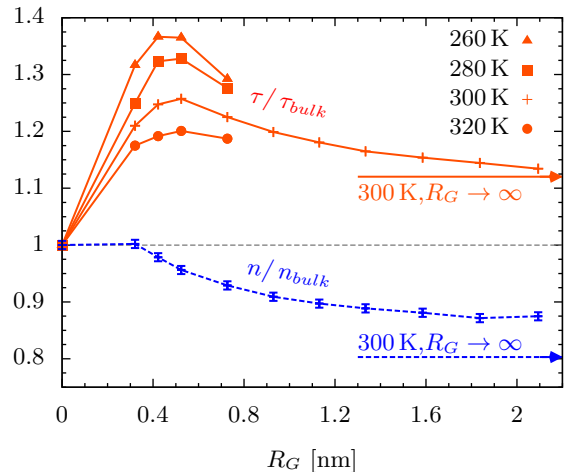


Fig. 5: Mean hydrogen bond (HB) lifetime of first-solvation shell water $\tau(R_G)$ versus solute size scaled by the bulk value τ_{bulk} (orange symbols). Average number of HBs per water molecule $n(R_G)$ scaled by its bulk value n_{bulk} (blue symbols). The values corresponding to the respective measures at the limiting case of zero curvature ($R_G \rightarrow \infty$, only $T = 300$ K) are drawn as horizontal arrows with respective color coding. The errorbars for n/n_{bulk} were estimated from block averages as described in the SI.

separation of initially bonded water molecule pairs after HB breaking. Without this separation, breaking a HB between two water molecules is reversible and the kinetics associated with this process are much faster than the irreversible rearrangements of the water hydrogen bond network analyzed here [42]. The correlation functions and details on the H-bond definition and numerical evaluation can be found in the SI.

The results for $\tau(R_G)$ scaled by their bulk value $\tau_{bulk} = 3.4$ ps are plotted in Fig. 5. They exhibit a non-monotonic size dependence with a maximum retardation of about 25% versus bulk at roughly $R_G \simeq 0.45$ nm, close to the structural crossover length scale. After the maximum, the retardation decreases for solute sizes $R_G > 0.5$ nm down to a remaining $\approx 5\%$ near the planar surface. Concurrently, the average number of HBs per water molecule n/n_{bulk} , also shown in Fig. 5, decreases monotonically. Hence, the non-monotonic translational mobility behavior of water is solely reflected in the kinetic behavior of the HBs. The observed behavior reconciles previous, apparently contradicting results from simulations [28] and theory [29, 30] on water reorientation times, as we find both predicted trends (increasing and decreasing life times), but in different solute size regimes, roughly separated by the important structural crossover scale.

Fig. 5 also plots the T -dependence on the HB correlation times where a significant slowing down with decreasing temperature can be observed with not much change of the position of the maximum on the solute-size axis.

We note that the latter behavior cannot be related one-to-one to our observed diffusivity behavior in (Fig 3) due to the multiple timescales entering τ ([42] and SI).

In summary, we have established a firm link between structure and dynamics of hydration water around hydrophobic solutes with a novel dynamic anomaly happening at the well-know crossover length scale. Due to the fundamental importance of surface water to biomolecular processes and function [16, 26], in particular at topologically heterogeneous protein surfaces [19–21, 27], our findings imply that nature has the means to employ local surface topology to mediate biological function. Hence, our results will help in the interpretation of experimentally found dynamic heterogeneities on biomolecular surfaces [16–21]. Locally slowed down water, for instance, could thus fine-tune the folding kinetics of hydrophobic polymers and peptides [16] or may mediate the appropriate time scales for the association of ligands to catalytically active sites or binding pockets [16, 22, 45].

The authors thank Roland R. Netz for helpful discussions and the Deutsche Forschungsgemeinschaft (DFG) for financial support. M. Heyden is grateful for support by the Cluster of Excellence RESOLV (EXC 1069) funded by the Deutsche Forschungsgemeinschaft.

* To whom correspondence should be addressed. E-mail: joachim.dzubiella@helmholtz-berlin.de

- [1] D. Chandler, *Nature* **437**, 640 (2005).
- [2] C. Y. Lee, J. A. McCammon, and P. J. Rossky, *J. Chem. Phys.* **80**, 4448 (1984).
- [3] A. Nicholls, K. A. Sharp, and B. Honig, *PROTEINS: Struct. Funct. Gen.* **11**, 281 (1991).
- [4] K. Lum, D. Chandler, and J. D. Weeks, *J. Phys. Chem. B* **103**, 4570 (1999).
- [5] D. M. Huang, P. L. Geissler, and D. Chandler, *J. Phys. Chem. B* **105**, 6704 (2001).
- [6] D. M. Huang and D. Chandler, *J. Phys. Chem. B* **106**, 2047 (2002).
- [7] S. Rajamani, T. M. Truskett, and S. Garde, *Proc. Natl. Acad. Sci. (USA)* **102**, 9475 (2005).
- [8] H. S. Ashbaugh and L. R. Pratt, *Rev. Mod. Phys.* **78**, 159 (2006).
- [9] L. R. Pratt, *Ann. Rev. Phys. Chem.* **53**, 409 (2002).
- [10] Y. S. Djikaev and E. Ruckenstein, *J. Chem. Phys.* **139**, 184709 (2013).
- [11] J. G. Davis, K. P. Gierszal, P. Wang, and D. Ben-Amotz, *Nature* **491**, 582 (2012).
- [12] B. J. Berne, J. D. Weeks, and R. Zhou, *Annu. Rev. Phys. Chem.* **60**, 85 (2009).
- [13] D. M. Huang and D. Chandler, *Proc. Natl. Acad. Sci. (USA)* **97**, 8324 (2000).
- [14] M. V. Athawale, G. Goel, T. Ghosh, T. M. Truskett, and S. Garde, *Proc. Natl. Acad. Sci. (USA)* **104**, 733 (2007).
- [15] I. T. S. Li and G. C. Walker, *Proc. Natl. Acad. Sci. (USA)* **108**, 1652716532 (2012).
- [16] B. Bagchi, *Chemical Reviews* **105**, 3197 (2005).
- [17] G. Niehus, M. Heyden, D. A. Schmidt, and M. Havenith, *Faraday Discuss.* **150**, 193 (2011).
- [18] O. H. Kwon, T. H. Yoo, C. M. Othon, J. A. V. Deventer, D. A. Tirrell, and A. H. Zewail, *Proc. Natl. Acad. Sci. (USA)* **107**, 17101 (2010).
- [19] L. Zhang, L. Wang, Y.-T. Kao, W. Qiu, Y. Yang, O. Okobiah, and D. Zhong, *Proc. Natl. Acad. Sci. (USA)* **104**, 18461 (2007).
- [20] F. Pizzitutti, M. Marchi, F. Sterpone, and P. J. Rossky, *J. Phys. Chem. B* **111**, 7584 (2007).
- [21] A. C. Fogarty and D. Laage, *J. Phys. Chem. B* **118**, 7715 (2014).
- [22] P. Setny, R. Baron, P. Kekenes-Huskey, J. A. McCammon, and J. Dzubiella, *Proc. Natl. Acad. Sci. (USA)* **110**, 1197 (2013).
- [23] J. Mittal and G. Hummer, *Proc. Natl. Acad. Sci. (USA)* **105**, 20130 (2008).
- [24] S. Vaikuntanathan and P. L. Geissler, *Phys. Rev. Lett.* **112**, 020603 (2014).
- [25] A. J. Patel, P. Varilly, S. N. Jamadagni, H. Acharya, S. Garde, and D. Chandler, *Proc. Natl. Acad. Sci. U.S.A.* **108**, 17678 (2011).
- [26] S. N. Jamadagni, R. Godawat, and S. Garde, *Annu. Rev. Chem. Biomol. Eng.* **2**, 147 (2011).
- [27] Y. K. Cheng and P. J. Rossky, *Nature* **392**, 696–699 (1998).
- [28] P. L. Chau, T. R. Forester, and W. Smith, *Molecular Physics* **89**, 1033 (1996).
- [29] D. Laage, G. Stirnemann, and J. T. Hynes, *J. Phys. Chem. B* **113**, 2428 (2009).
- [30] N. Galamba, *J. Phys. Chem. B* **118**, 4169 (2014).
- [31] H. S. Ashbaugh, *Chem. Phys. Lett.* **477**, 109–111 (2009).
- [32] H. J. C. Berendsen, J. R. Grigera, and T. P. Straatsma, *J. Phys. Chem.* **91**, 6269 (1987).
- [33] B. Hess, C. Kutzner, D. van der Spoel, and E. Lindahl, *J. Chem. Theory Comput.* **4**, 435 (2008).
- [34] A. Gosh, J. Samuel, and S. Sinha, *EPL* **98**, 30003 (2012).
- [35] P. Kumar, S. V. Buldyrev, F. W. Starr, N. Giovambattista, and H. E. Stanley, *Phys. Rev. E* **72**, 051503 (2005).
- [36] M. Hinczewski, Y. von Hansen, J. Dzubiella, and R. R. Netz, *J. Chem. Phys.* **132**, 245103 (2010).
- [37] F. Seldmeier, Y. von Hansen, L. Mengyu, D. Horinek, and R. R. Netz, *J. Stat. Phys.* **145**, 240 (2011).
- [38] G. H. Weiss, *Adv. Chem. Phys.* **13**, 1 (1966).
- [39] Y. Rosenfeld, *Phys. Rev. A* **15**, 6 (1977).
- [40] M. Dzugasov, *Nature* **381**, 137 (1996).
- [41] A. Luzar and D. Chandler, *Nature* **379**, 55 (1996).
- [42] A. Luzar, *J. Chem. Phys.* **113**, 23 (2000).
- [43] O. Markovitch and N. Agmon, *J. Chem. Phys.* **129**, 084505 (2008).
- [44] R. G. Pereyra, A. J. B. di Lorenzo, D. C. Malaspina, and M. A. Carignano, *Chemical Physics Letters* **538**, 35 (2012).
- [45] M. Grossman, B. Born, M. Heyden, D. Tworowski, G. B. Fields, I. Sagi, and M. Havenith, *Nature Struct. Biol.* **18**, 1103 (2011).

Supporting Information for: "Curvature Dependence of Hydrophobic Hydration Dynamics"

R. Gregor Weiß,^{1,2} Matthias Heyden,³ and Joachim Dzubiella^{1,2,*}

¹*Department of Physics, Humboldt Universität zu Berlin,
Newtonstr. 15, D-12489 Berlin, Germany, Germany*

²*Soft Matter and Functional Materials, Helmholtz-Center Berlin,
Hahn-Meitner Platz 1, D-14109 Berlin, Germany*

³*Max-Planck-Institut für Kohlenforschung, Kaiser-Wilhelm-Platz 1, D-45470 Mülheim an der Ruhr, Germany*

Molecular Dynamics Simulations

The systems comprise SPC/E water as solvent and a single hydrophobic sphere fixed in the middle of the simulation box. The interaction between SPC/E and the model solute is mediated by a shifted Lennard Jones potential $U_{LJ}(r') = 4\epsilon[(\sigma/r')^{12} - (\sigma/r')^6]$ whereas $r' = r - r_0$ increases the solute size. The parameters $\epsilon = 1.197$ kJ/mol and $\sigma = 3.768$ Å are those of a united-atom methane molecule as in Ref.[1]. Ten separate simulations are performed with shift radii $r_0 = 0$ Å, 1 Å, 2 Å, 4 Å, 6 Å, 8 Å, 10 Å, 12.5 Å, 15 Å and 17.5 Å. For shift radii $r_0 \leq 6$ Å the simulation box contains 6000 SPC/E water molecules and for simulations with $r_0 > 6$ Å the number of solute molecules is doubled to 12000 to avoid finite size effects.

To model the corresponding hydrophobic surface without curvature the walls in the x-y-plane of a simulation box of size $5.67 \times 5.67 \times 6.54$ nm³ are set to interact with water with a 12-6 potential in the z-direction $U_{12-6}(z) = 4\epsilon[(\sigma/z)^{12} - (\sigma/z)^6]$ with same interaction parameters $\epsilon = 1.197$ kJ/mol and $\sigma = 3.768$ Å.

Each system is equilibrated in NPT ensemble for 100 ps at ambient conditions, namely $T = 300$ K and $P = 1$ bar. After equilibration the box lengths of the cubic boxes are roughly 5.65 nm and 7.15 nm for the small (6000 SPC/E) and big (12000 SPC/E) setups respectively. In order to gather enough statistics to probe long-time dynamics within the thin solvation shell comprised of $\mathcal{O}(10)$ to $\mathcal{O}(10^2)$ water molecules subsequent production runs have a length of 200 ns for the small systems and 100 ns for the big systems with a time step of 2 fs and writing period of 200 fs. Energy divergence is prevented by simulation in NVT ensemble ($T = 300$ K) applying the Nosé-Hoover thermostat with a coupling period of 1 ps. The Nosé-Hoover is implemented by an extra degree of freedom introduced as a heat bath within the hamiltonian of the simulation and thus has the advantage of creating physically more realistic NVT ensembles [5, 6].

Additional simulations for the cavities with $r_0 = 0$ Å, 1 Å, 2 Å and 4 Å were performed in order to resolve the temperature dependence of our observations. Production runs with $T = 260$ K, 280 K and 320 K were performed up to 100 ns.

All simulations are performed with the GROMACS 4.5.4 package [4].

Planar Limit

The spatial distribution function in figure 1 of water at planar walls with the interaction parameters mentioned above does not exhibit a clear first and second minimum. The missing extrema hinder a clear definition of a first and second solvation shell as it can be observed from the RDFs (main text Fig. 1) for curved surfaces.

One further simulation of a wall interacting with a doubled interaction strength $\epsilon = 2.394$ kJ/mol was conducted to generate clear extrema (Fig. 1) and hence definitions for the solvation layers. Clearly, the found borders to the solvation shells only approximate values that correspond to values that would consistently define hydration layers for the original interaction parameters.

Another notable difference to simulations of water at curved surfaces arises from the lack of long-range correction for the interaction in the planar geometry. This creates smaller water densities and larger mobilities than in bulk [3].

Both discrepancies introduce minor consistency deviations between the simulations with the curved surfaces and the planar limit but never conflict with our interpretation.

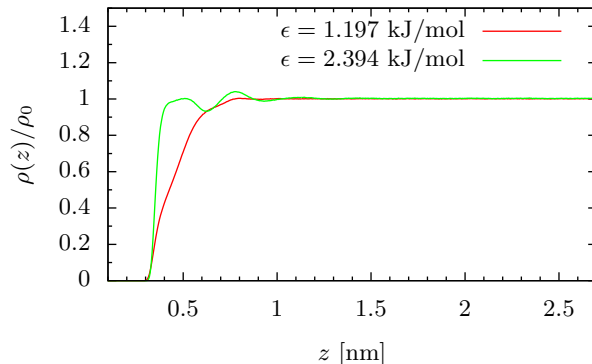


Fig. 1: Normalized water distribution at hydrophobic walls.

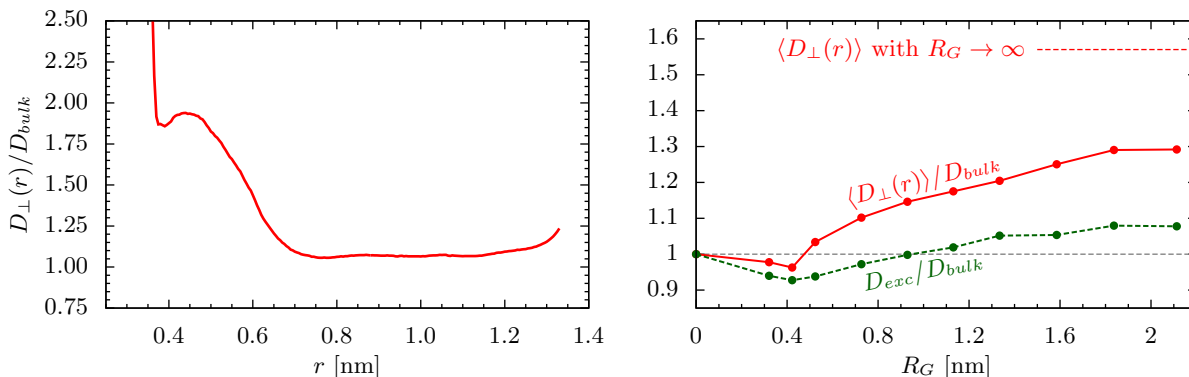


Fig. 2: Left panel: Spatially resolved perpendicular diffusion profile of water at the hydrophobic wall. Right panel: (red, solid) Average perpendicular diffusion constant $\langle D_{\perp}(r) \rangle$ (eq. 1) inside the solvation layer of differently sized hydrophobic model solutes. The red horizontally dashed line is the corresponding value at the planar limit ($R_G \rightarrow \infty$) for $\langle D_{\perp}(r) \rangle$ (green, dashed) Excess perpendicular diffusion constant $D_{exc} + 1$ (eq. 2) quantifying an average disruption of the diffusion of water near hydrophobic solutes. The reference value of bulk diffusivity is drawn as grey horizontally dashed line as isoline with value 1.

MFPT method and perpendicular diffusivity

In the main text we briefly describe the MFPT method from Hinczewski *et al.* [2] which takes the free energy profile $F(r)$ and the spatial derivative of the MFPT curve $T_{fp}(r, r_t)$. Both are obtained equivalently to the application of pair diffusion of water and methane by Sedlmeier *et al.* [3]. The integral $\int_{r_{min}}^r dr e^{-\beta F(r)}$ is evaluated numerically starting from the reflective boundary r_{min} , which we define by the largest distance from the respective solute where $F(r_{min}) \geq 10 k_B T$. The derivative $\partial T_{fp}(r, r_t) / \partial r$ is determined by fitting a linear function to the function values around $r - \delta r < r < r + \delta r$ whereas $\delta r = 0.05$ nm. The closest distance r evaluated for the derivative, and hence diffusivity profile value closest to the solute, is $r \lesssim R_G$ where statistics of $T_{fp}(r, r_t)$ allow a reasonable fit in the mentioned range of δr .

The left panel of Fig.2 plots the diffusivity profile of water motion perpendicular to the hydrophobic planar model surface. The diffusivity right at the surface decreases rapidly from high mobility values to a global minimum proceeding into a maximum which is located within the hydration water layer. With growing distance to the wall the diffusivity then decreases to bulk diffusion. The minimum at the outer margin of the solvation shell which is visible in each profile in Fig.4 of the main text almost fully vanishes for the profile of the planar surface here.

The right panel in Fig.2 shows two further measures quantifying the perpendicular diffusivity in vicinity of the hydrophobic model solutes. The red curve is an average diffusivity inside the first solvation shell

$$\langle D_{\perp}(r) \rangle = \int_{R_{max}}^{R_1} dr g_{so}(r) \cdot D_{\perp}(r) . \quad (1)$$

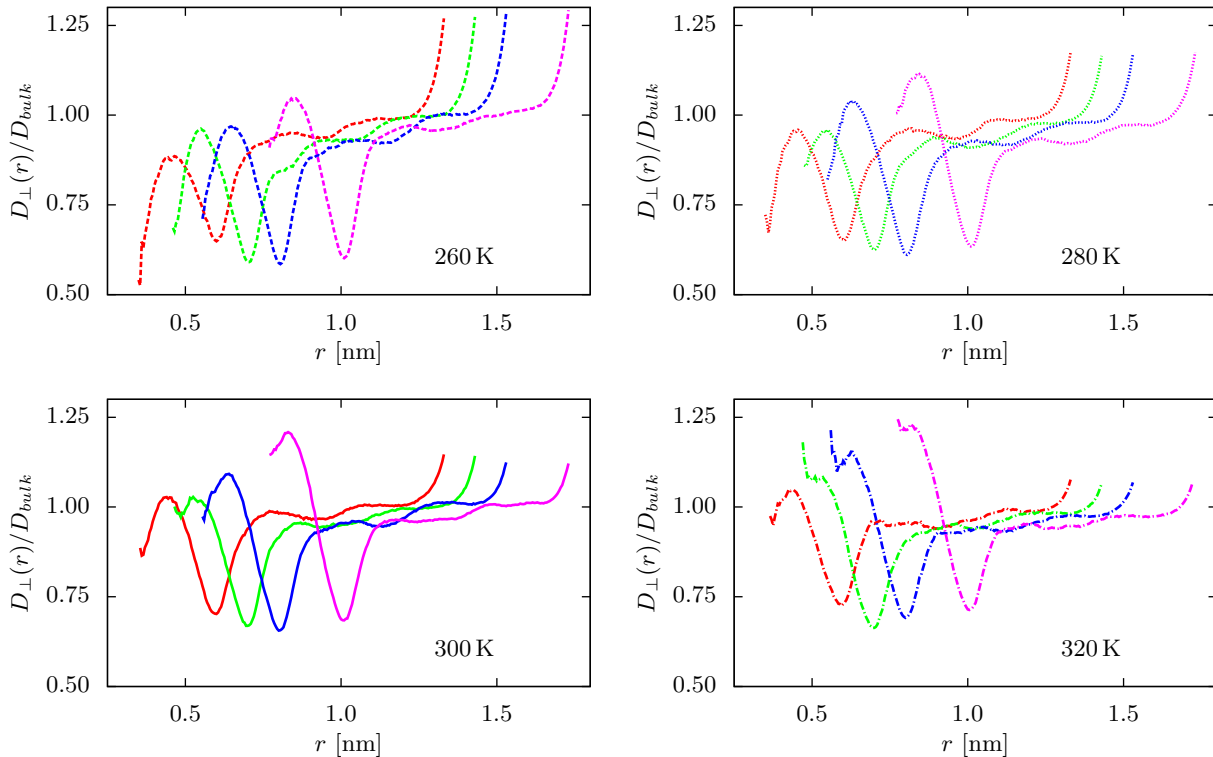


Fig. 3: Perpendicular diffusion at cavities with $r_0 = 0 \text{ \AA}$, 1 \AA , 2 \AA and 4 \AA with temperatures $T = 260 \text{ K}$ (upper left), $T = 280 \text{ K}$ (upper right), $T = 300 \text{ K}$ (bottom left) and $T = 320 \text{ K}$ (bottom right).

It captures the non-monotonicity from the diffusivity profiles slightly decreasing below bulk diffusion near small solutes and subsequently increases converging towards the value for perpendicular diffusion at the planar interface.

We also calculate an "excess" perpendicular diffusivity D_{exc} which quantifies an average change of the diffusivity constant in the solute's surrounding water

$$D_{exc} = \int_{R_{max}}^{\infty} dr r^2 g_{so}(r) \cdot [D_{\perp}(r)/D_{bulk} - 1] . \quad (2)$$

The plot shows $1 + D_{exc}(R_G)$. Certainly the non-monotonic curvature dependence in the diffusivity profiles is smoothly captured in this quantity as well. In general an excess diffusivity constant can be of particular interest in order to estimate water diffusivity changes in dilute solutions of hydrophobic solutes.

Hydrogen Bond Time Correlation

We analyse the autocorrelation function $c(t)$ of the H-bond existence inside the first hydration layer using an in-house analysis code. It uses a geometric H-bond definition with a minimum donor-acceptor distance $d_{HB} \leq 3.5 \text{ \AA}$ and donor-hydrogen-acceptor angle $\theta_{HB} \geq 150^\circ$.

Fig. 4 plots the correlation functions $c(t)$ for hydrogen bonds inside the first hydration layer. Hydrogen bonds were selected at time 0 if they were intact and both, acceptor and donor molecules, resided in the first hydration shell. We evaluate $c(t)$ up to correlation times of 100 ps until when it has decayed to magnitudes of 10^{-3} . Therefore, the integral over the correlation function in this time window provides a reasonable lower boundary to the actual HB lifetimes.

In addition the average number of hydrogen bonds per water molecule n within the solvation layer was counted and presented in the main text. The error of the average number of hydrogen bonds per molecule is estimated by block averaging. Using a frequency of a 1000 ps the average number of hydrogen bonds within a block of 100 ps length was

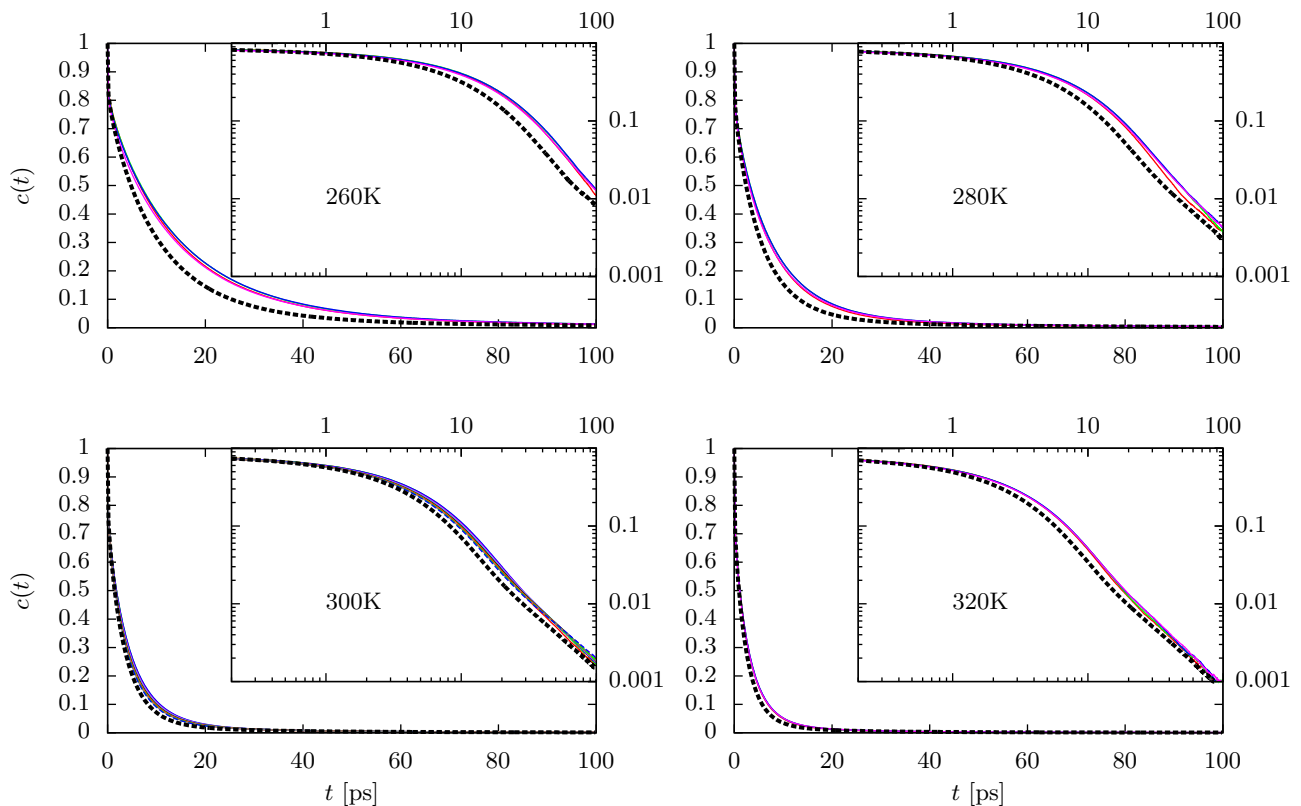


Fig. 4: Correlation function $c(t)$ of the hydrogen bonding operator $h(t)$ of hydrogen bonds on water molecules inside the first solvation shell with temperatures $T = 260$ K (upper left), $T = 280$ K (upper right), $T = 300$ K (bottom left) and $T = 320$ K (bottom right). Only at $T = 300$ K all cavity sizes were evaluated. For the rest the analysis was limited to cavities with $r_0 = 0 \text{ \AA}$, 1 \AA , 2 \AA and 4 \AA .

calculated, giving 100 uncorrelated block averages n_{Block} . These were used to approximate the standard deviation error by $\delta n = [\sum_{Blocks} (n - n_{Block})^2 / 100]^{1/2}$.

Temperature dependence of hydrogen bond dynamics

The hydrogen bond correlation function $c(t)$ contains all three time scales of the reaction-diffusion model from Luzar and Chandler [7] given by

$$\begin{aligned} \frac{\partial}{\partial t} \rho(\vec{r}, t) &= D \nabla^2 \rho(\vec{r}, t) + \delta(\vec{r}) k c(t) - \delta(\vec{r}) k' n(t) \\ &\equiv D \nabla^2 \rho(\vec{r}, t) + k(t) \delta \vec{r}, \end{aligned}$$

where the rates k and k' are those for breaking and reformation of a hydrogen bond, respectively. $n(t)$ is proportional to the diffusivity since $n(t) \propto \rho(0, t)$ [8] (and $\rho(r, t)$ obeying Fick's law).

Thus, as we used the reactive flux $k(t) = -\dot{c}(t)$ to evaluate the *zero frequency part*

$$\tau = \int c(t) dt = \int \frac{k(t) + k' n(t)}{k} dt,$$

the correlation time τ contains the factor Dk'/k , which precludes a direct one-to-one connection to the temperature dependence of the diffusivity. Certainly a direct relation of temperature dependence between hydrogen bond dynamics and diffusivity is restored if the time scales were extracted separately, which, however, is not a straightforward task.

* To whom correspondence should be addressed. E-mail: joachim.dzubiella@helmholtz-berlin.de

- [1] D. M. Huang and D. Chandler, *J. Phys. Chem. B* **106**, 2047 (2002).
- [2] M. Hinczewski, Y. von Hansen, J. Dzubiella and R. R. Netz, *J. Chem Phys* **132**, 245103 (2010).
- [3] F. Sedlmeier, Y. von Hansen, L. Mengyu, D. Horinek and R. R. Netz, *J. Stat. Phys.* **145**, 240 (2011).
- [4] B. Hess, C. Kutzner, D. van der Spoel and E. Lindahl, *J. Chem. Theory Comput.* **4**, 435 (2008).
- [5] S. Nosé, *J. Chem. Phys.* **81**, 511 (1984).
- [6] W. G. Hoover, *Physical Review A* **31**, 1695 (1985).
- [7] A. Luzar and D. Chandler, *Nature* **379**, 55 (1996).
- [8] A. Luzar, *J. Chem. Phys.* **113**, 23 (2000).